

Self-assembly of Human Galectin-1 via dual supramolecular interactions and its inhibition of T-cell agglutination and apoptosis

Wenjing Qi¹, Yufei Zhang¹, Zdravko Kochovski², Jue Wang¹, Yan Lu^{2,3}, Guosong Chen¹ (✉), and Ming Jiang¹

¹The State Key Laboratory of Molecular Engineering of Polymers and Department of Macromolecular Science, Fudan University, Shanghai 200438, China

²Soft Matter and Functional Materials, Helmholtz-Zentrum Berlin für Materialien und Energie, Berlin 14109, Germany

³Institute of Chemistry, University of Potsdam, 14476 Potsdam, Germany

Received: 20 June 2018

Revised: 2 August 2018

Accepted: 3 August 2018

© Tsinghua University Press and Springer-Verlag GmbH Germany, part of Springer Nature 2018

KEYWORDS

protein self-assembly, supramolecular interactions, galectin, cell agglutination

ABSTRACT

Recently, we proposed a new strategy to construct artificial plant protein assemblies, which were induced by adding a small molecule, based on dual supramolecular interactions. In this paper, we further explored this method by employing Human Galectin-1 (Gal-1) as a building block to form self-assembled microribbons. Two non-covalent interactions, including lactose–lectin binding and dimerization of Rhodamine B (RhB), induced by the small molecule ligand addition, were involved in the crosslinking of the animal protein, resulting in the formation of assemblies. By using transmission electron microscopy (TEM), cryo-electron microscopy (cryo-EM), and three-dimensional (3D) tomographic analysis, we arrived at a possible mechanistic model for the microribbon formation. Furthermore, the morphology of protein assemblies could be fine-tuned by varying the incubation time, the protein/ligand ratio, and the chemical structures of ligands. Interestingly, the formation of protein microribbons successfully inhibited Gal-1 induced T-cell agglutination and apoptosis. This is because the multivalent and dynamic interactions in protein assemblies compete with the binding between Gal-1 and the glycans on cell surfaces, which suppresses the function of Gal-1 in promotion of tumor progression and metastasis.

1 Introduction

Proteins in living organisms often exist as sophisticated, assembled arrays with different morphologies. The ubiquitous natural protein assemblies, such as clathrin cages (zero-dimensional (0D)) [1], actin filaments

(one-dimensional (1D)) [2], and bacterial S-layers (two-dimensional (2D)) [3] are essential for various biological functions, including material and energy transportation. Inspired by these fascinating regular protein assemblies, great efforts have been made in laboratories to develop artificial protein assemblies

Address correspondence to guosong@fudan.edu.cn

[4]. Using the biological route of genetic protein engineering requires rigorous geometric design and tedious protein fabrication. Thus, in the past decades, supramolecular interactions have been applied to construct artificial protein assemblies [5, 6], in addition to the genetic engineering, which include metal coordination [7, 8], host–guest interactions [9, 10], and hydrophobic interactions [11]. Elaborate man-made protein nanostructures from nanowires, nanorings, and helical tubes to three-dimensional (3D) structures have been reported [12–14]. However, the enormous structural complexity of proteins makes the controlled self-assembly, especially large-size regular structures, still a long-lasting challenge.

Recently, we proposed and demonstrated that by using a small synthetic ligand which contains saccharide and rhodamine (RhB) groups, some proteins could self-assemble into 3D crystals [15], microtubes [16], and nanosheets [17]. The process was generally driven by protein–sugar interactions and π – π stacking of RhB. In the previous reports, the protein building blocks were limited to plant lectins such as concanavalin A (Con A) and soybean agglutinin (SBA), which have limited biological applications while forming assemblies. Thus, in this paper we aimed to study the self-assembly of animal lectins with various functions.

Human Galectin, a member of the family of mammalian lectins, has a highly conserved carbohydrate recognition domain (CRD) with an affinity to β -galactosides [18]. By recognizing specific saccharides on target cells, Human Galectin regulates a broad spectrum of cellular responses, such as proliferation, apoptosis, differentiation, adhesion, cytokine secretion progression, and immune responses [19–21]. As the most abundantly expressed homo-dimeric member in the galectin family, Human Galectin-1 (Gal-1) [22] was chosen in this work as a promising building block for self-assembly. Based on the dual supramolecular interactions, well-defined protein microribbons were achieved by the addition of a predetermined lactose-containing ligand. Furthermore, Gal-1 has been reported to be overexpressed in cancer cells and to bind to lactosides expressed on the surface of T cells, which causes T cell agglutination and apoptosis, weakening the anti-tumor immune response [23]. In our case, the inducing ligand acts as an efficient

competitor, leading to the formation of protein microribbons and then successfully inhibiting Gal-1 induced T cell agglutination.

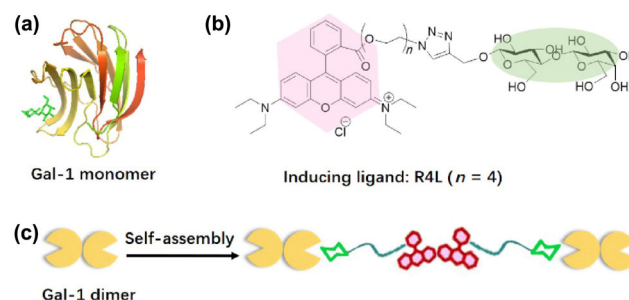
2 Results and discussion

2.1 Structure of the protein building block and the inducing ligands

Gal-1 is a well-known homodimer (each monomer 14.5 kDa) and consists of two CRDs [24]. As shown in Scheme 1(a), each monomer has one identical sugar-binding site that can specifically capture β -D-galactopyranoside containing saccharides. The inducing ligand R4L (Scheme 1(b)) was designed (synthetic procedures and characterizations are given in the Electronic Supplementary Material (ESM)) with three moieties including (1) a sugar unit of lactose (L), which is capable of specific binding to Gal-1, (2) RhB (R), which is responsible for ligand dimerization due to the π – π stacking, and (3) a short oligo (ethylene oxide) spacer with tunable length ($n = 4$) connecting the lactose with RhB. Scheme 1(c) describes the dual supramolecular interactions during the protein assembly. Two Gal-1 could be connected through the molecular recognition between the lectin and sugar and the π – π stacking of RhB between the neighboring ligands.

2.2 Preparation and characterization of the protein microribbons

By incubating Gal-1 (70 μ M) with R4L (210 μ M) in phosphate buffered saline (PBS) buffer at 4 $^{\circ}$ C for 24 h,



Scheme 1 (a) Structure of Gal-1 monomer. The filled space model represents lactose (shown in green) binding region (structure adapted from reported crystal structure, Protein Databank accession code: 1GZW). (b) Chemical structure of the inducing ligand R4L. (c) Specific recognition between Gal-1 and R4L with RhB dimerization while being tethered to protein.

protein microribbons formed as observed under the transmission electron microscopy (TEM). (Fig. 1(a)) The protein ribbons have a micrometer-scale length and a width of around 150 nm. The formation of such protein assemblies in solution was confirmed using dynamic light scattering (DLS) analysis (Fig. 1(b)). Furthermore, atomic force microscopic (AFM) image in Fig. 1(c) revealed the height of the microribbons was about 11 nm, indicating a multilayer structure as the size of Gal-1 dimer is ca. 2 nm × 2 nm × 5.5 nm. In the tomographic reconstruction (Fig. 1(d)), protein protofilaments of 2 nm in width packed into well-organized microribbons were clearly observed. The packing of single protein nanofilaments was further confirmed by using cryo-electron microscopy (cryo-EM) analysis (Fig. 1(e)).

In addition, to verify the dual supramolecular interactions in the protein assemblies, the specific

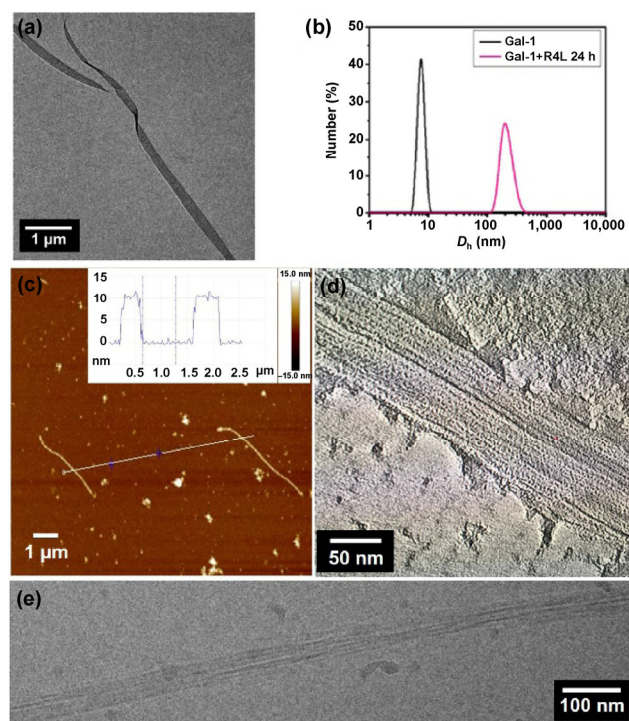


Figure 1 (a) TEM image of Gal-1/R4L protein microribbons. TEM samples were negatively stained and air-dried on carbon grids. (b) DLS results of Gal-1/R4L solution (Gal-1: 70 μM, R4L: 210 μM) after incubation for 24 h at 4 °C. (c) AFM image of Gal-1/R4L protein microribbons. (d) A 0.46 nm thick XY tomographic slice from an electron tomogram of a Gal-1/R4L protein microribbon consisting of protein protofilaments. TEM samples were negatively stained and air-dried on carbon grids. (e) Cryo-EM image of a Gal-1/R4L protein microribbon.

recognition between Gal-1 and lactose was confirmed by isothermal titration calorimetry (ITC) measurements (Fig. S1 in the ESM). The binding constant was measured as 4.5×10^{-4} M, which is consistent with the published data [25]. The dimerization of RhB was also confirmed by ultraviolet–vis (UV–vis) absorption spectra and circular dichroism (CD) spectra. The peak at 525 nm was obviously enhanced as a signal of RhB dimerization in Gal-1/R4L mixture when compared to free ligands (Fig. S2 in the ESM).

In order to gain further insight on how dimeric Gal-1 assembled into microribbons, 3D tomography was performed to display the inner structure of the microribbons. As shown in Fig. 2(a), regular aligned patterns of protofilaments were observed. Interestingly, the corresponding isosurface representation (Fig. 2(b)) indicated that the protofilaments exhibit a wave-like structure with a repeating unit of 11 nm, corresponding to the size of two connected Gal-1 dimers. The tomographic images of the well-packed wave-like protein assemblies and the corresponding isosurface representations with different magnifications and angles were also supplied in Fig. S3 in the ESM. The wave-like property of the protofilaments could be attributed to the specific pseudo-symmetric dimerization mode of Gal-1 [26]. The two sugar-binding sites

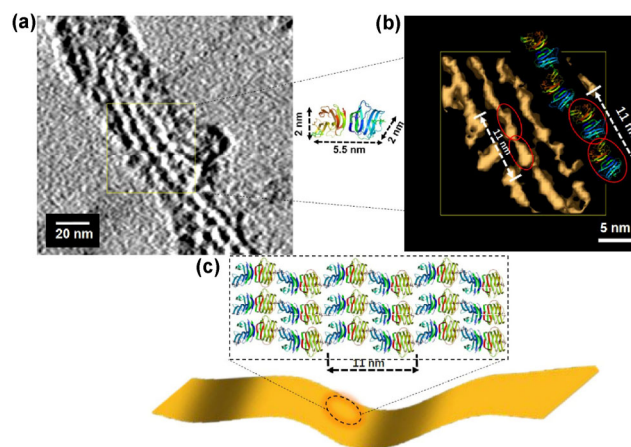


Figure 2 (a) A 0.46 nm thick XY tomographic slice from an electron tomogram of negatively stained protein microribbon. Inset: structure of Human Gal-1 dimer adapted from reported crystal structure, Protein Databank accession code: 1GZW. (b) Isosurface representation of protein microribbon, the red circle represents one Gal-1 dimer, two dimers packed as a repeating unit in the protofilament. (c) A plausible protein packing mode in microribbons.

of Gal-1 are pseudo-symmetric: The two identical monomers were related by a 2-fold rotation axis so it favors the formation of wave-like filamentary assemblies and 2D ribbons. A plausible packing in protein ribbons was proposed as shown in Fig. 2(c). Firstly, the dual supramolecular interactions of lactoside–lectin specific recognition and the dimerization of RhB induced wave-like protofilaments formation. Secondly, the asymmetric binding sites not only contributed to wave-like filaments, but also made protein filaments interact with each other to generate the 2D protein ribbons.

2.3 Controllable growth of the protein microribbons

The growth of the protein ribbons could be controlled by the incubation time. As shown in Fig. 3, after incubating the proteins with the excessive ligands (3 equiv.) for 8 h, protein ribbon precursors (protofilaments) were observed with a width less than 100 nm. After 24 h, the width of the ribbons increased to around 500 nm and kept growing until 2 weeks later when a width around 1 μm was achieved. Even in such a large protein assembly, well-defined packing of the proteins can be preserved and observed by using cryo-EM as shown in Fig. S4 in the ESM. Then we found that prolonged incubation time would not result in widening the protein ribbon formation further. Figure 3(b) shows the width distribution of the protein ribbons observed by TEM. DLS analysis was also performed to detect the variation of ribbons in solutions vs. time (Fig. S5 in the ESM).

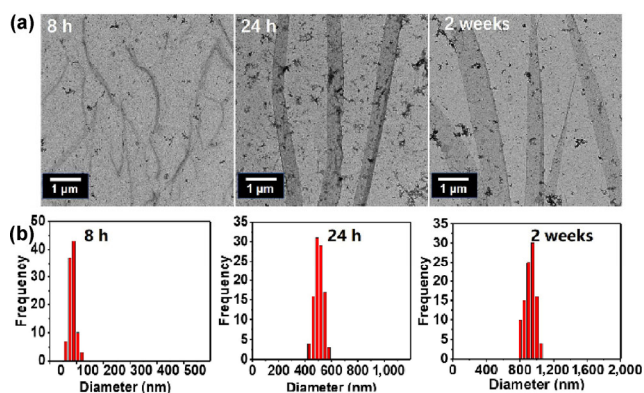


Figure 3 (a) TEM images of time-dependent protein ribbons obtained at different incubation time. TEM samples were negatively stained and air-dried on carbon grids. (b) Width distributions of protein ribbons observed by TEM at different time intervals.

The growth and yield of protein ribbons could also be tuned by different protein/ligand ratios. The sizes of protein ribbons with different protein/ligand ratios were compared after incubation for two weeks. As shown in Fig. 4, when the protein/ligand ratio was 1:3 (70 μM /210 μM), the average width of protein ribbons was about 1 μm . However, if we fixed the concentration of protein and increased the protein/ligand ratios to 1:1 and 3:1, the average widths of the protein ribbons were increased to 2 and 5 μm , respectively. In the meantime, the yield of protein ribbons became less as ligand decreased. Such ratio-controlled size variation also helped us understand the kinetic control of the protein ribbon formation better. Herein, the ligand was considered a crucial “seed” to crosslink dimeric Gal-1. When the concentration of protein was kept constant, the excessive ligands (protein/ligand ratio was 1:3) would generate more protein protofilaments at the very beginning of the incubation. Therefore, more ribbons grew at the same time, leading to slender ribbon formation. On the other hand, if there were less “seeds” in the solution (protein/ligand ratios of 1:1 and 3:1), the number of ribbon precursors decreased, so that more free proteins could assemble on the same ribbon resulting in wider protein ribbons. The protein/ligand ratio-controlled self-assembly can also be proven by the dimerization efficiency of ligands. By using UV–vis and CD (Fig. S7 in the ESM), an equal concentration of protein and ligand (1:1) showed the highest dimerization efficiency.

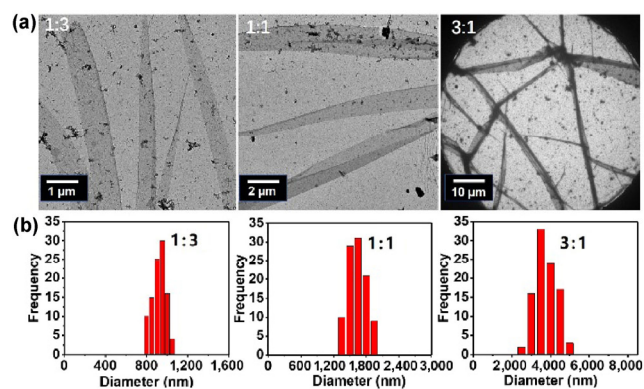


Figure 4 (a) TEM images of microribbons obtained by using different protein/ligand ratios (1:3, 1:1 and 3:1 respectively). TEM samples were negatively stained and air-dried on carbon grids. All images were achieved after incubating the protein and R4L for 2 weeks. (b) Width distributions of protein ribbons observed by TEM at different protein/ligand ratios.

In our previous reports [17], a slight change in the linker length of the ligand resulted in various morphologies of plant protein assemblies. Thus, in this work, the length of the tether in RnL was changed by tuning the number of ethylene oxide repeating units ($n = 1, 2, 3, 4, 5$). It was found that despite different spacer lengths, RnL always induced the formation of Gal-1 protein ribbons without distinguishable morphologies. However, when lactoside was replaced by galactoside, the designed ligand R1G induced the formation of protein microwires with a uniform width of 25 nm (Fig. 5) and a height about 2 nm (Fig. S8 in the ESM) as an indication of monolayer protein assembly. According to the crystal structures of Gal-1-ligand (Fig. S9 in the ESM, Protein Databank accession code: 1W6O and 1W6M), the electron density of galactopyranoside in Gal-1-lactosides matches well with that in Gal-1-galactose. This means that the carbohydrate parts share similar configuration in both lactose and galactose. Thus, besides the EG linker, the difference between disaccharide and monosaccharide also induced morphology change of the protein assembly. In short, R1G, with the shortest length, resulted in the formation of protein microwires while longer ligands such as RnL favored ribbon formation.

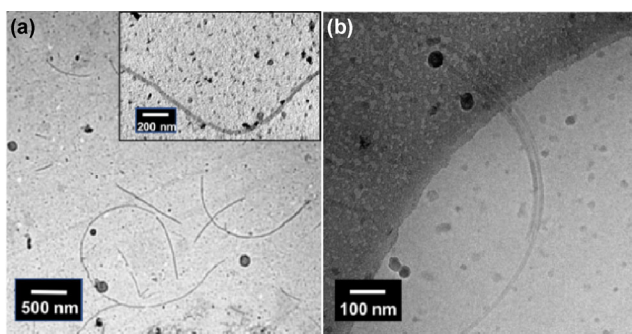


Figure 5 (a) TEM images of Gal-1/R1G protein nanowires. TEM samples were negatively stained and air-dried on carbon grids. (b) Cryo-EM image of Gal-1/R1G protein nanowires.

2.4 Protein assemblies induced inhibition of T-cell agglutination

Gal-1 has arisen as a key mediator in many cellular responses. For example, excess Gal-1 binds to lactosides present on T cell surfaces, acting as bivalent factors and then nucleates cell agglutination, finally resulting in

the apoptosis of T cells [27]. As shown in Fig. S10 in the ESM, Jurkat cells were incubated with different concentrations of Gal-1. Time-dependent and dose-dependent cell agglutination was visualized by microscopic images. When Jurkat cells were incubated with Gal-1 (500 $\mu\text{g}/\text{mL}$) for 4 h, obvious cell agglutination was observed. We were curious whether the formation of microribbons could attenuate this agglutination by accommodating the distal binding sites of Gal-1 through multivalent interactions. To that end, first, the formation of protein microribbons in cell culture media (RPMI 1640) at 37 $^{\circ}\text{C}$ was confirmed by TEM in Fig. S11 in the ESM. Second, different concentrations of ligands (R4L) were added to induce Gal-1 microribbon formation and the inhibition of cell agglutination was investigated by confocal fluorescence microscopic analysis.

As shown in Fig. 6(a), obvious cell agglutination was observed while Jurkat cells were incubated with Gal-1 (500 $\mu\text{g}/\text{mL}$) for 4 h. With increasing concentrations of ligand to protein, cell agglutination was inhibited gradually. However, the added free lactose did not inhibit cell agglutination efficiently even at a high concentration. Furthermore, the inhibition efficiency can be quantitatively assessed by automatic cell counts. More cell agglutination (less free cells) leads to a lower cell count in the automatic cell count analysis so the cell agglutination can be quantified (further illustration in Fig. S12 in the ESM). As shown in Fig. 6(b), 500 $\mu\text{g}/\text{mL}$ Gal-1 without ligands dramatically induced the cells agglutination leading to the lowest cell count compared to the control groups (PBS group and ligand group). The inhibition efficiency was directly correlated to ligand concentration with an increasing cell count, finally saturating at 15 equiv. However, the addition of 20 equiv. free lactose showed a comparative cell count to the Gal-1 group and could not inhibit cell agglutination as efficiently as ligands did. The phenomenon occurs because the ligand acts as an efficient competitor through multivalent interactions. The interactions between Gal-1 and lactosides on the T cell surface would have been surpassed and replaced by the competitive ligands, which favors protein assembly formation through multivalent interactions. In addition, successful

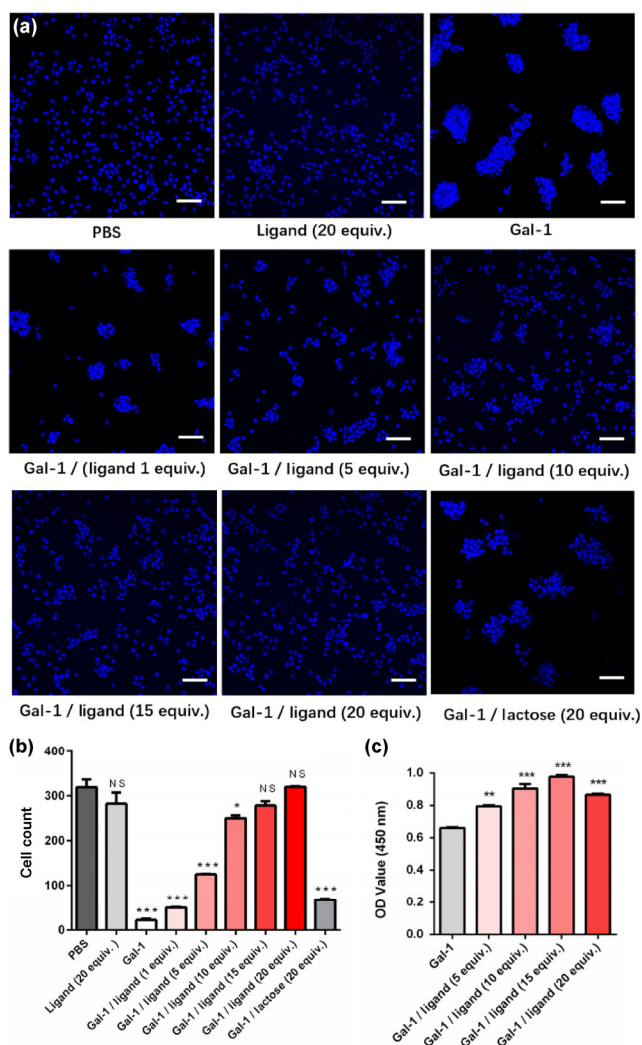


Figure 6 (a) Confocal fluorescence microscopic images of cell agglutination: successful inhibition of Jurkat cell agglutination with Gal-1 (500 $\mu\text{g}/\text{mL}$) in the presence of ligands (from 17 $\mu\text{g}/\text{mL}$, 1 equiv. to 340 $\mu\text{g}/\text{mL}$, 20 equiv.) and 20 equiv. lactose as control. Scale bar = 50 μm . (Jurkat cells: 0.05 million/well) (b) Automatic cell count was performed by image J to quantify the cell agglutination [28]. (c) Jurkat cell viability assay with Gal-1 (500 $\mu\text{g}/\text{mL}$) in the presence of ligands (5 equiv. to 20 equiv.) (CCK-8). Results are shown as means \pm standard error of mean (SEM) as indicated. Statistical significance was calculated by One-way ANOVA (compared to PBS group). * $p < 0.05$, ** $p < 0.01$, *** $p < 0.001$.

inhibition of Jurkat cell apoptosis (Fig. 6(c) and Fig. S13 in the ESM) with Gal-1 (500 $\mu\text{g}/\text{mL}$) by the addition of ligands indicates that the ligands have the ability to accommodate distal binding sites of Gal-1 through multivalent interactions, which eventually inhibit T cell agglutination and the agglutination-induced T cell apoptosis.

3 Conclusion

In summary, for the first time to the best of our knowledge, Human Galectin was found to be able to generate protein microribbons. Based on the protein-carbohydrate interactions and the dimerization of RhB, wave-like protein protofilaments were formed with a packing mode of two Gal-1 dimers as a first repeating unit, followed by further assembly of the protofilaments into protein microribbons. These protein microribbons could multivalently and dynamically accommodate the binding between Gal-1 and cell receptors and inhibit T-cell agglutination and apoptosis, which offers a viable therapeutic avenue for the treatment of T-cell proliferation.

Acknowledgements

We acknowledge the financial support from the National Natural Science Foundation of China (Nos. 51721002, 21504016, and 91527305). We thank Joint Lab for Structural Research at the Integrative Research Institute for the Sciences (IRIS Adlershof, Berlin) for Cryo-TEM imaging.

Electronic Supplementary Material: Supplementary material (experimental section including synthetic details of ligands, preparation procedures of protein assemblies and characterization data) is available in the online version of this article at <https://doi.org/10.1007/s12274-018-2169-7>.

References

- [1] Fotin, A.; Cheng, Y. F.; Sliz, P.; Grigorieff, N.; Harrison, S. C.; Kirchhausen, T.; Walz, T. Molecular model for a complete clathrin lattice from electron cryomicroscopy. *Nature* **2004**, *432*, 573–579.
- [2] Pollard, T. D.; Cooper, J. A. Actin, a central player in cell shape and movement. *Science* **2009**, *326*, 1208–1212.
- [3] Sára, M.; Sleytr, U. B. S-Layer proteins. *J. Bacteriol.* **2000**, *182*, 859–868.
- [4] Garcia-Seisdedos, H.; Empereur-Mot, C.; Elad, N.; Levy, E. D. Proteins evolve on the edge of supramolecular self-assembly. *Nature* **2017**, *548*, 244–247.
- [5] Luo, Q.; Hou, C. X.; Bai, Y. S.; Wang, R. B.; Liu, J. Q. Protein assembly: Versatile approaches to construct highly ordered nanostructures. *Chem. Rev.* **2016**, *116*, 13571–13632.

- [6] Bai, Y. S.; Luo, Q.; Liu, J. Q. Protein self-assembly via supramolecular strategies. *Chem. Soc. Rev.* **2016**, *45*, 2756–2767.
- [7] Sinclair, J. C. Self-assembly: Proteins on parade. *Nat. Chem.* **2012**, *4*, 346–347.
- [8] Brodin, J. D.; Smith, S. J.; Carr, J. R.; Tezcan, F. A. Designed, helical protein nanotubes with variable diameters from a single building block. *J. Am. Chem. Soc.* **2015**, *137*, 10468–10471.
- [9] Hou, C. X.; Li, J. X.; Zhao, L. L.; Zhang, W.; Luo, Q.; Dong, Z. Y.; Xu, J. Y.; Liu, J. Q. Construction of protein nanowires through cucurbit[8]uril-based highly specific host-guest interactions: An approach to the assembly of functional proteins. *Angew. Chem., Int. Ed.* **2013**, *52*, 5590–5593.
- [10] Nguyen, H. D.; Dang, D. T.; van Dongen, J. L. J.; Brunsveld, L. Protein dimerization induced by supramolecular interactions with cucurbit[8]uril. *Angew. Chem., Int. Ed.* **2010**, *49*, 895–898.
- [11] Oohora, K.; Burazerovic, S.; Onoda, A.; Wilson, Y. M.; Ward, T. R.; Hayashi, T. Chemically programmed supramolecular assembly of hemoprotein and streptavidin with alternating alignment. *Angew. Chem., Int. Ed.* **2012**, *51*, 3818–3821.
- [12] Matsunaga, R.; Yanaka, S.; Nagatoishi, S.; Tsumoto, K. Hyperthin nanochains composed of self-polymerizing protein shackles. *Nat. Commun.* **2013**, *4*, 2211.
- [13] Zhang, W.; Luo, Q.; Miao, L.; Hou, C. X.; Bai, Y. S.; Dong, Z. Y.; Xu, J. Y.; Liu, J. Q. Self-assembly of glutathione S-transferase into nanowires. *Nanoscale* **2012**, *4*, 5847–5851.
- [14] Staples, J. K.; Oshaben, K. M.; Horne, W. S. A modular synthetic platform for the construction of protein-based supramolecular polymers via coiled-coil self-assembly. *Chem. Sci.* **2012**, *3*, 3387–3392.
- [15] Sakai, F.; Yang, G.; Weiss, M. S.; Liu, Y. J.; Chen, G. S.; Jiang, M. Protein crystalline frameworks with controllable interpenetration directed by dual supramolecular interactions. *Nat. Commun.* **2014**, *5*, 4634.
- [16] Yang, G.; Zhang, X.; Kochovski, Z.; Zhang, Y. F.; Dai, B.; Sakai, F.; Jiang, L.; Lu, Y.; Ballauff, M.; Li, X. M.; Liu, C.; Chen, G. S.; Jiang, M. Precise and reversible protein-microtubule-like structure with helicity driven by dual supramolecular interactions. *J. Am. Chem. Soc.* **2016**, *138*, 1932–1937.
- [17] Yang, G.; Ding, H. M.; Kochovski, Z.; Hu, R. T.; Lu, Y.; Ma, Y. Q.; Chen, G. S.; Jiang, M. Highly ordered self-assembly of native proteins into 1D, 2D, and 3D structures modulated by the tether length of assembly-inducing ligands. *Angew. Chem., Int. Ed.* **2017**, *56*, 10691–10695.
- [18] Rabinovich, G. A.; Toscano, M. A. Turning “sweet” on immunity: Galectin-glycan interactions in immune tolerance and inflammation. *Nat. Rev. Immunol.* **2009**, *9*, 338–352.
- [19] Argüeso, P.; Panjwani, N. Focus on molecules: Galectin-3. *Exp. Eye Res.* **2011**, *92*, 2–3.
- [20] Perillo, N. L.; Pace, K. E.; Seilhamer, J. J.; Baum, L. G. Apoptosis of T cells mediated by galectin-1. *Nature* **1995**, *378*, 736–739.
- [21] He, J. L.; Baum, L. G. Endothelial cell expression of galectin-1 induced by prostate cancer cells inhibits T-cell transendothelial migration. *Lab. Invest.* **2006**, *86*, 578–590.
- [22] Tribulatti, M. V.; Figini, M. G.; Carabelli, J.; Cattaneo, V.; Campetella, O. Redundant and antagonistic functions of galectin-1, -3, and -8 in the elicitation of T cell responses. *J. Immunol.* **2012**, *188*, 2991–2999.
- [23] Disney, M. D.; Childs-Disney, J. L. “Supra”molecular recognition of galectin 1. *Chem. Biol.* **2007**, *14*, 1095–1097.
- [24] Thiemann, S.; Baum, L. G. Galectins and immune responses—Just how do they do those things they do? *Annu. Rev. Immunol.* **2016**, *34*, 243–264.
- [25] Nesmelova, I. V.; Ermakova, E.; Daragan, V. A.; Pang, M.; Menéndez, M.; Lagartera, L.; Solís, D.; Baum, L. G.; Mayo, K. H. Lactose binding to galectin-1 modulates structural dynamics, increases conformational entropy, and occurs with apparent negative cooperativity. *J. Mol. Biol.* **2010**, *397*, 1209–1230.
- [26] López-Lucendo, M. F.; Solís, D.; André, S.; Hirabayashi, J.; Kasai, K. I.; Kaltner, H.; Gabius, H. J.; Romero, A. Growth-regulatory human galectin-1: Crystallographic characterisation of the structural changes induced by single-site mutations and their impact on the thermodynamics of ligand binding. *J. Mol. Biol.* **2004**, *343*, 957–970.
- [27] Belitsky, J. M.; Nelson, A.; Hernandez, J. D.; Baum, L. G.; Stoddart, J. F. Multivalent interactions between lectins and supramolecular complexes: Galectin-1 and self-assembled pseudopolyrotaxanes. *Chem. Biol.* **2007**, *14*, 1140–1151.
- [28] Grishagin, I. V. Automatic cell counting with ImageJ. *Anal. Biochem.* **2015**, *473*, 63–65.